Introduction

In regions with complex structure, wave-equation depth migration is a powerful tool for accurately imaging the earth's interior. The quality of the image depends on the quality of the velocity model and on the quality of the technique used for wavefield reconstruction in the subsurface. Structural imaging is not the only objective of wave-equation imaging. We often seek to construct images depicting reflectivity as a function of reflection angles. Such images highlight the subsurface illumination patterns, and could be used for amplitude variation with angle analysis and for tomography.

Angle gathers can be produced with ray methods (Brandsberg-Dahl et al., 2003) or with wavefield methods (de Bruin et al., 1990; Sava and Fomel, 2003; Biondi and Symes, 2004; Xu et al., 2010). Such gathers have similar characteristics, although ray-based angle gathers are hampered by artifacts caused by the asymptotic assumptions (Stolk and Symes, 2004). Angle decomposition can be applied before or after the imaging condition. The methods implemented before the imaging condition are costly since they operate on complex wavefields characterized by multipathing. The methods operating after the imaging condition are more efficient and decompose images represented as a function of space and extensions (Rickett and Sava, 2002; Sava and Fomel, 2006; Sava and Vasconcelos, 2010).

Angle-domain imaging uses common-image-gathers (CIGs) describing the reflectivity as a function of angles and a space axis (depth). We can construct common-image-point-gathers (CIP) selected at various positions in the subsurface. As pointed out by Sava and Vasconcelos (2010), CIPs are advantageous because they sample the image at the most relevant locations (along the main reflectors), they avoid computations at unhelpful locations (inside salt bodies), they can have variable density depending on the complexity of the structure and reliability of the image, and they avoid the bias of gathers constructed as a function of the depth axis.

Here we focus on angle imaging using CIPs constructed with 3D wide-azimuth data. Such data pose challenges for angle-domain imaging, mainly arising from the large data size and the interpretation difficulty of data of higher dimensionality. Several techniques have been proposed for wide-azimuth angle decomposition, including ray-based methods (Koren et al., 2008) and wavefield methods using wavefield decomposition before imaging (Xu et al., 2010) or after imaging (Sava and Fomel, 2003). Here, we discuss angle gather construction using extended CIPs. This technique is applicable for any type of wave-equation imaging, including reverse-time migration.

Wide-azimuth angle-domain imaging

In conventional seismic imaging, waves originating at the source propagate into the medium (the source wavefield), interact with the discontinuities (reflectors) and return to the surface as reflected waves (the receiver wavefield) (Berkhout, 1982). Waves that do not interact with reflectors are excluded from this model. Imaging is a process involving two steps: the reconstruction of the source and receiver wavefields and the imaging condition applied to the reconstructed wavefields. Since the two wavefields coincide kinematically at discontinuities, an imaging condition can be formulated as the zero lag of their cross-correlation (Clærbout, 1985):

$$R(\mathbf{x}) = \sum_{shots} \sum_{t} W_s(\mathbf{x}, t) W_r(\mathbf{x}, t) \ , \tag{1}$$

where R represents the migrated image, $\mathbf{x} = \{x, y, z\}$ and t is time.

An extended imaging condition preserves in the output image acquisition or illumination parameters. In shot-record migration, the source and receiver wavefields are reconstructed on the same computational grid at all locations in space and all times or frequencies, therefore there is no a-priori wavefield separation that can be transferred to the output image. The separation can be constructed by correlation of the wavefields from symmetric locations relative to the image point, measured in space and time:

$$R(\mathbf{x}, \boldsymbol{\lambda}, \tau) = \sum_{shots} \sum_{t} W_s(\mathbf{x} - \boldsymbol{\lambda}, t - \tau) W_r(\mathbf{x} + \boldsymbol{\lambda}, t + \tau) \ . \tag{2}$$

Assuming that all errors accumulated in the wavefields are due to the velocity model, the extended images could be used for velocity model building by exploiting semblance or focusing properties (Yang

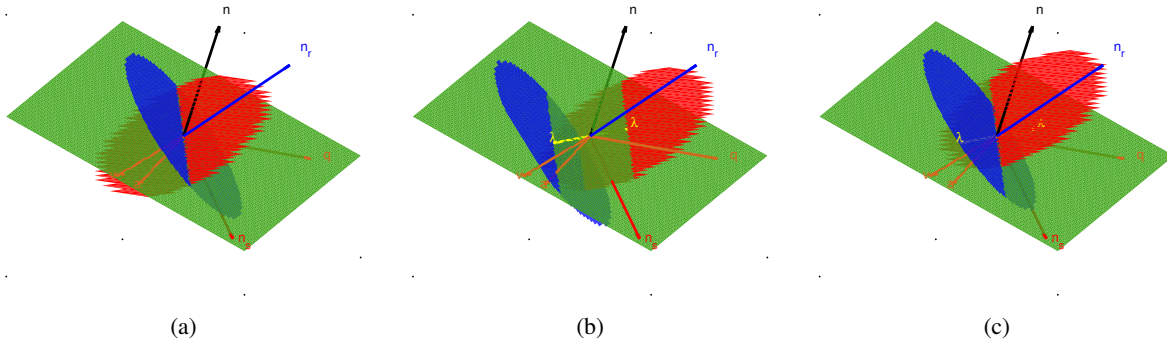(a)   (b)   (c)

Figure 1: (a) The source/receiver planes in their original position, i.e. as obtained by wavefield reconstruction. (b) The source/receiver planes displaced with the space-lag $\boldsymbol{\lambda}$ constrained in the reflector plane. (c) The source/receiver planes displaced with space-lag $\boldsymbol{\lambda}$ and time-lag τ.

and Sava, 2010). Here, we are discussing the decomposition of extended CIPs as a function of azimuth ϕ and reflection θ angles at selected points in the image. We derive the moveout function characterizing reflections in extended CIPs and illustrate the technique with the SEAM 3D wide-azimuth synthetic.

An implicit assumption made by all methods of angle decomposition is that we can describe the reflection process by locally planar objects. Such methods assume that (locally) the reflector is a plane, and that the incident and reflected wavefields are also (locally) planar. Only with these assumptions we can define vectors in-between which we measure angles like the angles of incidence and reflection, as well as the azimuth angle of the reflection plane. Our method uses this assumption explicitly. We define the following unit vectors: $\mathbf{n}$, along the reflector normal; $\mathbf{a}$, the projection of the azimuth vector $\mathbf{v}$ in the reflector plane; $\mathbf{n}_s$ and $\mathbf{n}_r$, orthogonal to the source and receiver wavefronts; $\mathbf{q}$, at the intersection of the reflection plane and the reflector. The vectors $\mathbf{n}$, $\mathbf{n}_s$, $\mathbf{n}_r$ and $\mathbf{q}$ are co-planar and vectors $\mathbf{n}$ and $\mathbf{q}$ are orthogonal, Figure 1(a). Therefore, the (planar) source and receiver wavefields are given by the expressions:

$$\mathbf{n}_s \cdot \mathbf{x} = vt_s \quad and \quad \mathbf{n}_r \cdot \mathbf{x} = vt_r \ . \tag{3}$$

Here, t_s and t_r are times defining the planes under consideration, and v represents velocity at the image point. Equations 3 define the conventional imaging condition 1. This system states that an image is formed when the source and receiver wavefields are time-coincident at reflection points.

Similarly, we can rewrite the extended imaging condition 2 using the local approximation of the source and receiver wavefields:

$$\mathbf{n}_s \cdot (\mathbf{x} - \boldsymbol{\lambda}) = v(t_s - \tau) \quad and \quad \mathbf{n}_r \cdot (\mathbf{x} + \boldsymbol{\lambda}) = v(t_r + \tau) \ . \tag{4}$$

Here, v represents the local velocity at the image point. The source and receiver planes are shifted relative to one-another by equal quantities in the positive and negative directions and in space and time. We can eliminate the space variable $\mathbf{x}$ by substituting equations 3 in equations 4. By exploiting the fact that the normal vectors to the source and receiver planes and the normal to the reflector are related by Snell's law $\mathbf{n}_r = \mathbf{n}_s - 2(\mathbf{n}_s \cdot \mathbf{n})\mathbf{n}$, we obtain the system:

$$(\mathbf{q} \cdot \boldsymbol{\lambda})\sin\theta = v\tau \quad and \quad \mathbf{n} \cdot \boldsymbol{\lambda} = 0 \ . \tag{5}$$

Here, we use the fact that reflections occur only when $(\mathbf{n}_s \cdot \mathbf{n}) \neq 0$ and that $\mathbf{n}_s - (\mathbf{n}_s \cdot \mathbf{n})\mathbf{n} = \mathbf{q}\sin\theta$, and θ is the reflection angle contained in the reflection plane. Thus, the only space-lags that contribute to the extended image are those for which the space-lag vector $\boldsymbol{\lambda}$ is orthogonal to the reflector normal vector $\mathbf{n}$. Furthermore, assuming that the space-shift applied to the source and receiver planes is contained in the reflector plane, i.e. $\boldsymbol{\lambda} \perp \mathbf{n}$, then the first expression in 5 describe the moveout function in an extended gather as a function of the space-lag $\boldsymbol{\lambda}$, the time lag τ, the reflection angle θ, the orientation vector $\mathbf{q}$. The vector $\mathbf{q}$ is orthogonal to the reflector normal and depends on the reflection azimuth angle ϕ.

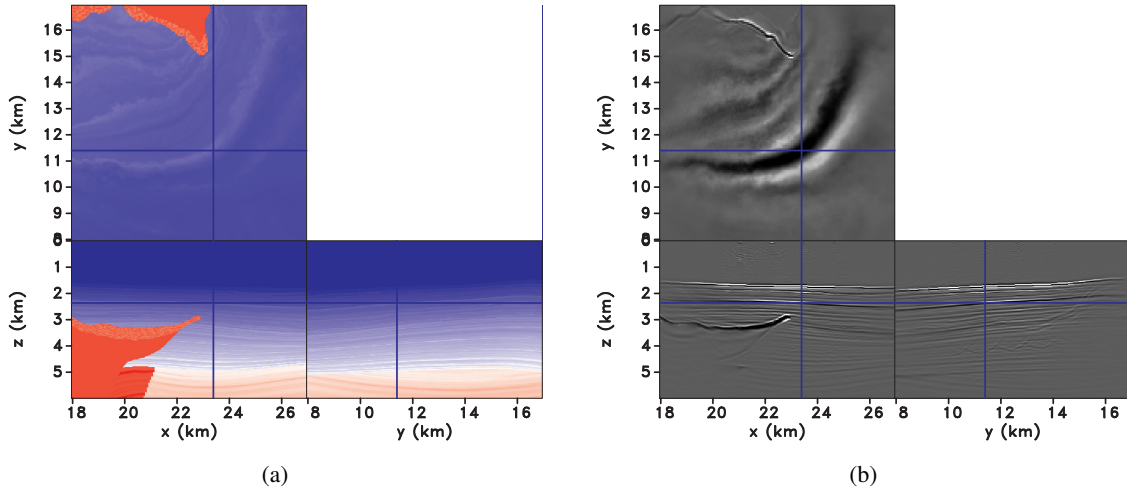
Figure 2: (a) A subset of the SEAM velocity model used for the imaging example in Figures 2(b)-3(c). (b) Conventional image obtained with the shots shown in Figure 3(a).

Figure 1(a) shows the source and receiver planes, and the reflector plane together with their unit vector normals. Figure 1(b) shows the source and receiver planes displaced by the space lag vector $\boldsymbol{\lambda}$ contained in the reflector plane, as indicated by equation 5. The displaced planes do not intersect at the reflection plane, thus they do not contribute to the extended image at this point. The time shift with the quantity $\tau = (\mathbf{q} \cdot \boldsymbol{\lambda}) \sin \theta / v$, i.e. a translation in the direction of plane normals, the source and receiver planes are restored to the image point, thus contributing to the extended image, Figure 1(c).

The angle decomposition of individual CIPs is independent of one-another, therefore the algorithm is easily parallelizable over the outer loop. At every CIP, we need to access the information about the reflector normal ($\mathbf{n}$) and about the local velocity (v). The reflector dip information can be extracted from the conventional image, and the velocity is the same as the one used for migration. Prior to the angle decomposition, we need to define a reference azimuth direction. Here, we define this azimuth direction using an arbitrary vector $\mathbf{v}$. Using the reflector normal ($\mathbf{n}$) we can build the projection of the azimuth vector ($\mathbf{a}$) in the reflector plane as $\mathbf{a} = (\mathbf{n} \times \mathbf{v}) \times \mathbf{n}$. In the following, we measure the azimuth angle ϕ relative to vector $\mathbf{a}$ and the reflection angle θ relative to the normal to the reflector given by vector $\mathbf{n}$.

Then, for every azimuth angle ϕ, using the reflector normal ($\mathbf{n}$) and the azimuth reference ($\mathbf{a}$), we can construct the trial vector $\mathbf{q}$ which lies at the intersection of the reflector and the reflection planes. We scan over all possible vectors $\mathbf{q}$, although only one azimuth corresponds to the reflection from a given shot. This scan ensures that we capture the reflection information from all shots in the survey. Given the reflector normal (the axis of rotation) and the trial azimuth angle ϕ, we can construct the different vectors $\mathbf{q}$ by the application of a rotation matrix by angle θ to the azimuth reference vector $\mathbf{a}$, i.e. $\mathbf{q} = Q(\mathbf{n}, \phi)\mathbf{a}$. For every reflection angle θ, we map the lag-domain CIP to the angle-domain by summation over the surface defined by equation 5. The output is the representation of the CIP in the angle-domain.

Example

We illustrate the method discussed in the preceding section with CIPs constructed using the wide-azimuth SEAM data. Figure 2(a) shows the velocity model. For demonstration, we consider 16 shots located at the locations of the thick dots in Figure 3(a). The large dot indicates the surface projection of the CIP used for illustration. We consider the azimuth reference vector oriented in the x direction, i.e. $\mathbf{v} = \{1, 0, 0\}$. Figure 3(b) shows the extended CIP obtained for all shots, and Figure 3(c) depicts its angle-domain decomposition. The circles indicating the reflection angles are drawn at every $5°$ and the radial lines indicating the azimuth directions are drawn at every $15°$. Given the sparse shot sampling, the CIP is sparsely illuminated, but at the correct reflection and azimuth angles.
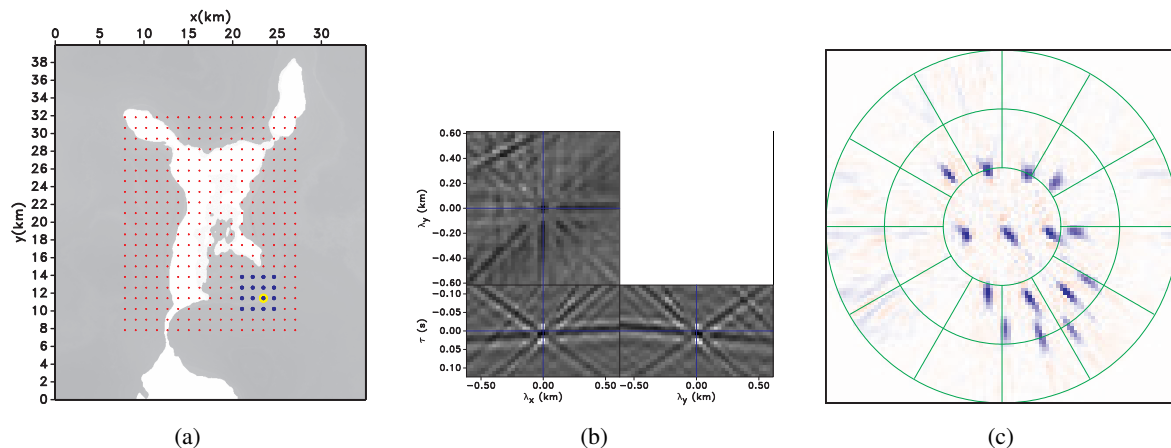
| (a) | (b) | (c) |

Figure 3: (a) The shots used for creating the image shown in Figure 2(b). (b) The extended image obtained for all shots, and (c) the corresponding angle-gather.

Conclusions

Angle decomposition with wavefield extrapolation is robust in complex geology and accurate in the presence of steeply dipping reflectors. Extended CIPs constructed at discrete image points provide sufficient information for angle decomposition. Both space- and the time-lag extensions are required to characterize the reflection geometry given by the local reflection and azimuth angles. Assuming that we know the reflector dip, we can avoid computing one component of the space-lag, thus increasing the computational efficiency of the method and making it affordable for large-scale wide-azimuth imaging projects.

Acknowledgments

REFERENCES

Berkhout, A. J., 1982, Imaging of acoustic energy by wave field extrapolation: Elsevier.

Biondi, B., and W. Symes, 2004, Angle-domain common-image gathers for migration velocity analysis by wavefield-continuation imaging: Geophysics, **69**, 1283–1298.

Brandsberg-Dahl, S., M. V. de Hoop, and B. Ursin, 2003, Focusing in dip and AvA compensation on scattering-angle/azimuth common image gathers: Geophysics, **68**, 232–254.

Clærbout, J. F., 1985, Imaging the Earth's interior: Blackwell Scientific Publications.

de Bruin, C. G. M., C. P. A. Wapenaar, and A. J. Berkhout, 1990, Angle-dependent reflectivity by means of prestack migration: Geophysics, **55**, 1223–1234.

Koren, Z., I. Ravve, E. Ragoza, A. Bartana, P. Geophysical, and D. Kosloff, 2008, Full-azimuth angle domain imaging: SEG Technical Program Expanded Abstracts, **27**, 2221–2225.

Rickett, J., and P. Sava, 2002, Offset and angle-domain common image-point gathers for shot-profile migration: Geophysics, **67**, 883–889.

Sava, P., and S. Fomel, 2003, Angle-domain common image gathers by wavefield continuation methods: Geophysics, **68**, 1065–1074.

———, 2006, Time-shift imaging condition in seismic migration: Geophysics, **71**, S209–S217.

Sava, P., and I. Vasconcelos, 2010, Extended imaging condition for wave-equation migration: Geophysical Prospecting, in press.

Stolk, C. C., and W. W. Symes, 2004, Kinematic artifacts in prestack depth migration: Geophysics, **69**, 562–575.

Xu, S., Y. Zhang, and B. Tang, 2010, 3D common image gathers from reverse time migration: SEG Technical Program Expanded Abstracts, **29**, 3257–3262.

Yang, T., and P. Sava, 2010, Moveout analysis of wave-equation extended images: Geophysics, **75**, 151–161.